

# Lattice Calculation of Pion Form Factor with Overlap Fermions

Gen Wang<sup>1,\*</sup>, Jian Liang<sup>1</sup>, Terrence Draper<sup>1</sup>, Keh-Fei Liu<sup>1</sup>, and Yi-Bo Yang<sup>2,3,4</sup>



(χQCD Collaboration)

<sup>1</sup>*Dept. of Physics and Astronomy, University of Kentucky, Lexington, KY 40506, USA*

<sup>2</sup>*CAS Key Laboratory of Theoretical Physics, Institute of Theoretical Physics, Chinese Academy of Sciences, Beijing 100190, China*

<sup>3</sup>*School of Fundamental Physics and Mathematical Sciences, Hangzhou Institute for Advanced Study, UCAS, Hangzhou 310024, China*

<sup>4</sup>*International Centre for Theoretical Physics Asia-Pacific, Beijing/Hangzhou, China*

We present a precise calculation of the pion form factor using overlap fermions on six ensembles of 2+1-flavor domain-wall configurations with pion masses varying from 137 to 339 MeV. Taking advantage of the fast Fourier transform and other techniques to access many combinations of source and sink momenta, we find the pion mean square charge radius to be  $\langle r_\pi^2 \rangle = 0.433(9)(13) \text{ fm}^2$ , which agrees with the experimental result, including the systematic uncertainties from chiral extrapolation, lattice spacing and finite volume dependence. We also find that  $\langle r_\pi^2 \rangle$  depends on both the valence and sea quark masses strongly and predict the pion form factor up to  $Q^2 = 1.0 \text{ GeV}^2$  which agrees with experiments very well.

**Introduction:** The electric form factor  $f_{\pi\pi}(Q^2)$ ,  $Q^2 \equiv -(p' - p)^2 \geq 0$ , is defined from the pionic matrix element and its slope at  $Q^2 = 0$  gives the mean square charge radius

$$\langle \pi^i(p') | V_\mu^j(0) | \pi^k(p) \rangle = i\epsilon^{ijk}(p_\mu + p'_\mu) f_{\pi\pi}(Q^2), \quad (1)$$

$$\langle r_\pi^2 \rangle \equiv -6 \frac{df_{\pi\pi}(Q^2)}{dQ^2} \Big|_{Q^2=0}, \quad (2)$$

where  $V_\mu^j = \bar{\psi} \frac{1}{2} \tau^j \gamma_\mu \psi$  is the isovector vector current,  $\tau^i$  are the Pauli matrices in flavor space, and  $|\pi^i\rangle$  are the pion triplet states.  $\langle r_\pi^2 \rangle$  has been determined precisely based on the existing  $\pi e$  scattering data [1–3] and  $e^+e^- \rightarrow \pi^+\pi^-$  data [4, 5] averaged by the Particle Data Group (PDG) [6] as  $\langle r_\pi^2 \rangle = 0.434(5) \text{ fm}^2$ . Phenomenologically,  $f_{\pi\pi}(Q^2)$  is fitted quite well over the range  $0 < Q^2/m_\rho^2 < 0.4$  with the single monopole form  $(1 + Q^2/\Lambda^2)^{-1}$ , with  $\Lambda \sim m_\rho$ . This gives credence to the idea of vector dominance [7, 8]. In chiral perturbation theory,  $\langle r_\pi^2 \rangle$  has been calculated with  $SU(2)$  Chiral Perturbation Theory [9] at NNLO and also at NLO with  $SU(3)$  formula [10], which entails the uncertainties of the low energy constants.

Since lattice QCD is an *ab initio* calculation and the experimental determination of  $\langle r_\pi^2 \rangle$  from the  $\pi e$  scattering is very precise, it provides a stringent test for lattice QCD calculations to demonstrate complete control over the statistical and systematic errors in estimates of the relevant pionic matrix element. Over the years, the pion form factor has been calculated with quenched approximation [11, 12], and for the  $N_f = 2$  [13–17],  $N_f = 2 + 1$  [18–23] and  $N_f = 2 + 1 + 1$  [24] cases.

In this work, we use valence overlap fermions to calculate the pion form factor on six ensembles of domain-wall fermion configurations with different sea pion masses, including two at the physical pion mass, four lattice spacings and different volumes to control the systematic errors. Due to the multi-mass algorithm available for overlap fermions, we can effectively calculate several valence quark masses on each ensemble [25–27] and also  $O(100)$  combinations of the initial and final pion momenta with little overhead with the usage of the fast Fourier transform (FFT) algorithm [28] in the three-point function contraction. This allows us to study both the sea and the valence quark mass dependence of  $\langle r_\pi^2 \rangle$  in terms of partially quenched chiral perturbative theory, besides giving an accurate result at the physical pion mass.

Lattice	$L^3 \times T$	$a$ (fm)	$La$ (fm)	$m_\pi$ (MeV)	$m_\pi L$	$n_{\text{cfg}}$
24IDc	$24^3 \times 64$	0.195	4.66	141	3.33	231
32ID	$32^3 \times 64$	0.143	4.58	172	3.99	199
32IDh	$32^3 \times 64$	0.143	4.58	250	5.80	100
48I	$48^3 \times 96$	0.114	5.48	139	3.86	81
24I	$24^3 \times 64$	0.111	2.65	340	4.56	202
32I	$32^3 \times 64$	0.083	2.65	302	4.05	309

TABLE I. The ensembles and their respective lattice size  $L^3 \times T$ , lattice spacing  $a$ , pion mass  $m_\pi$  and number of configurations  $n_{\text{cfg}}$ .

**Numerical details:** We use overlap fermions on six ensembles of HYP smeared 2+1-flavor domain-wall fermion configurations with Iwasaki gauge action (labeled with I) [29, 30] and Iwasaki plus the Dislocation Suppressing Determinant Ratio (DSDR) gauge action (labeled with ID) [31] as listed in Table I. The effective quark propagator of the massive overlap fermions is the inverse of the operator  $(D_c + m)$  [32, 33], where

\* genwang27@uky.edu

$D_c$  is chiral, i.e.,  $\{D_c, \gamma_5\} = 0$  [34]. And it can be expressed in terms of the overlap Dirac operator  $D_{ov}$  as  $D_c = \rho D_{ov}/(1 - D_{ov}/2)$ , with  $\rho = -(1/(2\kappa) - 4)$  and  $\kappa = 0.2$ . A multi-mass inveter is used to calculate the propagators with 2 to 6 valence pion masses varying from the unitary point to  $\sim 390$  MeV. On 24I, 32I and 24IDc (c stands for the coarse lattice spacing), Gaussian smearing [35] is applied with root mean square (RMS) radius 0.49 fm, 0.49 fm and 0.53 fm, respectively, for both source and sink. On 48I, 32ID and 32IDh (h for heavier pion mass), box-smearing [36, 37] with box half size 0.57 fm, 1.0 fm and 1.0 fm, respectively, is applied as an economical substitute for Gaussian smearing.

To extract pionic matrix elements, the three-point function (3pt)  $C_{3pt}(\tau, t_f, \vec{p}_i, \vec{p}_f)$  is computed,

$$C_{3pt} = \sum_{\vec{x}_f, \vec{z}} e^{-i\vec{p}_f \cdot \vec{x}_f} e^{-i\vec{q} \cdot \vec{z}} \langle \text{Tr}[\chi_{\pi^+}(x_f) V_4^3(z) \chi_{\pi^+}^\dagger(\mathcal{G})] \rangle \\ = \sum_{\vec{x}_f, \vec{z}} e^{-i\vec{p}_f \cdot \vec{x}_f} e^{-i\vec{q} \cdot \vec{z}} \langle \text{Tr}[\gamma_5 S(\mathcal{G}|z) \gamma_4 S(z|x_f) \gamma_5 S(x_f|\mathcal{G})] \rangle, \quad (3)$$

where  $\chi_{\pi^+}(\vec{x}, t) = \bar{d}(\vec{x}, t) \gamma_5 u(\vec{x}, t)$  is the interpolating field of the pion with  $u$  and  $d$  the up and down quark spinors,  $S(y|x)$  is the quark propagator from  $x$  to  $y$ ,  $z \equiv \{\tau, \vec{z}\}$ ,  $x_f \equiv \{t_f, \vec{x}_f\}$ ,  $\vec{p}_i$  and  $\vec{p}_f$  is the initial and final momentum of the pion, respectively,  $\vec{q} = \vec{p}_f - \vec{p}_i$  is the momentum transfer, and  $\mathcal{G}$  is the smeared  $Z_3$ -noise grid source [38]. The disconnected insertions in Eq.(3) vanish in the ensemble average [12].

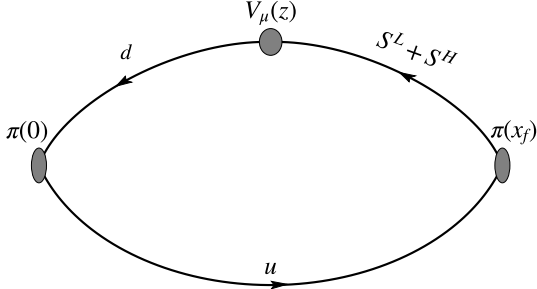


FIG. 1. Illustration of the pion three-point function with stochastic sandwich method. LMS is applied for the propagator between the current at  $z$  and the sink at  $x_f$  with FFT, but not for the propagators from the source at 0.

In practice,  $S(\mathcal{G}|z)$  in Eq. (3) is calculated with the  $\gamma_5$  hermiticity, i.e.,  $S(\mathcal{G}|z) = \gamma_5 S^\dagger(z|\mathcal{G}) \gamma_5$ , and  $S(z|x_f)$  is usually obtained in the sequential source method with  $\gamma_5 S(x_f|\mathcal{G})$  as the source [39, 40]. The calculation of the sequential propagators would need to be repeated for different  $\vec{p}_f$  and different quark mass  $m$ , so that the cost would be very high when dozens of momenta and multiple quark masses are calculated. Instead, we use the stochastic sandwich method [41, 42], but without low mode substitution (LMS) for  $S(x_f|\mathcal{G})$  since it is not efficient for pseudoscalar mesons [25]. However, the separation of sink position  $x_f$  and current position  $z$  in splitting the

low and high modes for the propagator  $S(z|x_f)$  between the current and sink can facilitate FFT along with LMS which is still useful here. As shown in Fig. 1,  $S(z|x_f)$  can be split into the exact low mode part based on the low lying overlap eigenvalues  $\lambda_i$  and eigenvectors  $v_i$  of the  $i$ th eigenmode of  $D_c$ , plus the noise-source estimate  $S_{\text{noi}}^H$  of the high mode part,

$$S(z|x_f) = S^L(z|x_f) + S^H(z|x_f), \\ S^L(z|x_f) = \sum_{\lambda_i \leq \lambda_c} \frac{1}{\lambda_i + m} v_i(z) v_i^\dagger(x_f), \quad (4) \\ S^H(z|x_f) = \frac{1}{n_f} \sum_{j=1}^{n_f} S_{\text{noi}}^H(z, \eta_j) \eta_j^\dagger(x_f),$$

where  $\lambda_c$  is the highest eigenvalue in LMS and is much larger than the quark mass  $m$  with the typical number of eigenmodes  $n_v \sim 200$  on 24I and 32I, and  $n_v \sim 900$  on 32ID, 32IDh, 24IDc and 48I; and  $S_{\text{noi}}^H(z, \eta_j)$  is the noise-estimated propagator for the high modes with the low-mode deflated  $Z_3$  noise  $\eta_j(x_f)$  [41, 42]. Sink smearing is applied on all the sink spatial points  $x_f$  of noise  $\eta_j(x_f)$  and eigenvectors  $v_i^\dagger(x_f)$ .

Thus  $C_{3pt}$  can be decomposed into factorized forms within the sums of the eigenmodes for the low modes and the  $n_f$  number of noises  $\eta_j$  for the high modes,

$$C_{3pt}(\tau, t_f, \vec{p}_i, \vec{p}_f) = \langle \sum_{\lambda_i \leq \lambda_c} \text{Tr}[\frac{1}{\lambda_i + m} G_i^L(\vec{q}, \tau) F_i^L(\vec{p}_f, t_f)] \\ + \sum_{j=1}^{n_f} \frac{1}{n_f} \text{Tr}[G_j^H(\vec{q}, \tau) F_j^H(\vec{p}_f, t_f)] \rangle, \quad (5)$$

where

$$G_i^L(\vec{q}, \tau) = \sum_{\vec{z}} e^{-i\vec{q} \cdot \vec{z}} \gamma_5 S(\mathcal{G}|z) \gamma_4 v_i(z), \quad (6)$$

$$F_i^L(\vec{p}_f, t_f) = \sum_{\vec{x}_f} e^{-i\vec{p}_f \cdot \vec{x}_f} v_i^\dagger(x_f) \gamma_5 S(x_f|\mathcal{G}), \quad (7)$$

$$G_j^H(\vec{q}, \tau) = \sum_{\vec{z}} e^{-i\vec{q} \cdot \vec{z}} \gamma_5 S(\mathcal{G}|z) \gamma_4 S_{\text{noi}}^H(z, \eta_j), \quad (8)$$

$$F_j^H(\vec{p}_f, t_f) = \sum_{\vec{x}_f} e^{-i\vec{p}_f \cdot \vec{x}_f} \eta_j^\dagger(x_f) \gamma_5 S(x_f|\mathcal{G}), \quad (9)$$

which are calculated by using FFTs on the spatial points  $\vec{z}$  and  $\vec{x}_f$  for each  $G_i^L$ ,  $F_i^L$ ,  $G_j^H$  and  $F_j^H$  to obtain any  $\vec{q}$  and  $\vec{p}_f$  with the computational complexity  $\mathcal{O}(V \log V)$  with  $V$  the lattice spatial volume. Compared with the stochastic sandwich method for a fixed  $\vec{p}_f$  which also includes the summation over the spatial points  $\vec{z}$  and  $\vec{x}_f$ , eigenvectors  $v_i$  and noises  $\eta_j$ , the additional cost factor of using FFTs  $\mathcal{O}(\log V)$  is only of order  $\sim 7$  for our largest 48I lattice. This allows us to calculate any combination of  $\vec{q}$  and  $\vec{p}_f$  without much additional cost compared to the traditional stochastic sandwich method.

**Analysis and results:** The source-sink separations  $t_f$  used in this work with different ensembles are collected in Table II. The largest  $t_f$  is  $\sim 2.0$  fm on the coarsest lattice 24IDc and the smallest one is  $\sim 0.7$  fm on the finest lattice 32I.

Lattice	$n_i$	$n_t$	$n_s$	$t_f/a$	$n_f$	$n_{\text{meas}}n_{\text{cfg}}$
24IDc	4	2	3	6, 7, 8, 9, 10	4, 4, 6, 4, 4	49896
32ID	6	2	2	9, 10, 11	4, 5, 12	19104
32IDh	6	2	2	9, 10, 11	4, 5, 12	9600
48I	5	3	4	8, 10, 12	4, 8, 12	77760
24I	8	1	2	10, 11, 12	3, 5, 5	12928
32I	8	1	2	8, 12, 15	4, 8, 12	19776

TABLE II. The lattice setup of this calculation. The  $n_i$  sets of smeared noise-grid sources with  $\{n_s, n_s, n_s, n_t\}$  points in  $\{x, y, z, t\}$  directions, respectively, are placed on the lattice to improve the statistics, and  $n_f$  sets of  $S_{\text{noi}}^H$  at  $2n_t$  sink time slices at  $i\frac{T}{n_t}t_f$  and  $T - i\frac{T}{n_t}t_f$  with  $i = \{1 \dots n_t\}$ . On a given configuration, the total number of the propagators we generated is  $n_i + n_f$  and  $n_{\text{meas}} = n_i n_s^3 n_t$  which is the number of measurements of 3pt.

There are two momentum setups used in this work: the special  $|\vec{p}_i| = |\vec{p}_f|$  case and the general  $|\vec{p}_i| \neq |\vec{p}_f|$  one. For the general momentum setup  $|\vec{p}_i| \neq |\vec{p}_f|$ , we parametrize the 3pt with momentum transfer  $\vec{q} = \vec{p}_f - \vec{p}_i$  by

$$\begin{aligned}
C_{3\text{pt}}(\tau, t_f, \vec{p}_i, \vec{p}_f) &= \frac{Z_{\vec{p}_i} Z_{\vec{p}_f} (E_i + E_f)}{E_i E_f Z_V} f_{\pi\pi}(Q^2) \\
&\times (e^{-E_i\tau - E_f(t_f - \tau)} + e^{-E_i(T/2 + \tau) - E_f(t_f - \tau)}) \\
&+ C_1 e^{-E_i\tau - E_f^1(t_f - \tau)} + C_2 e^{-E_i^1\tau - E_f(t_f - \tau)} \\
&+ C_3 e^{-E_i^1\tau - E_f^1(t_f - \tau)} + C_4 e^{-E_i(T/2 - t_f) - E_h(t_f - \tau)},
\end{aligned} \quad (10)$$

where  $Z_{\vec{p}}$  is the spectral weight and  $E$  and  $E^1$  is the ground state and first-excited state energy, respectively.  $Z_{\vec{p}_i}, Z_{\vec{p}_f}, E_i, E_f, E_i^1$  and  $E_f^1$  are constrained by the joint fit with the corresponding two-point function (2pt).  $Z_V$  is the finite normalization constant for the local vector current which is determined from the forward matrix element as  $Z_V \equiv \frac{2E}{\langle \pi(p) | V_4 | \pi(p) \rangle}$ .  $C_1, C_2$  and  $C_3$  are free parameters for the excited-state contaminations. Since we have put two sources at  $t = 0$  and  $t = T/2$  for most ensembles to increase statistics, we need a term with  $C_4$  and  $E_h$  to account for the case that the current insertion is outside of the time window between the source and the sink. The details of fittings are given in the supplementary materials [43].

For the special  $|\vec{p}_i| = |\vec{p}_f|$  case, one can simply calculate the ratio of 3pts, and obtain the pion form factor by the following parametrization of the ratio  $R_1$ ,

$$\begin{aligned}
R_1(\tau, t_f, \vec{p}_i, \vec{p}_f) &= C_{3\text{pt}}(\tau, t_f, \vec{p}_i, \vec{p}_f) / C_{3\text{pt}}(\tau, t_f, \vec{p}_i, \vec{p}_i) \\
&= f_{\pi\pi}(Q^2) + B_1(e^{-\Delta E\tau} + e^{-\Delta E(t_f - \tau)}) + B_2 e^{-\Delta E t_f},
\end{aligned} \quad (11)$$

where the terms with  $B_1$  and  $B_2$  are the contributions from the excited-state contamination, and  $\Delta E = E^1(\vec{p}_i) - E(\vec{p}_i)$  is the energy difference between the pion energy  $E(\vec{p}_i)$  and that of the first excited-state  $E^1(\vec{p}_i)$ . These energies are also constrained by the joint fit with the corresponding 2pt. Since the excited-state contaminations of the forward matrix element in the denominator are known to be small and the contribution from  $C_4$  term in Eq. (10) is suppressed by  $e^{-E(\vec{p}_i)T/2}$  with  $\vec{p}_i \neq \vec{0}$  for

both the denominator and numerator, we have dropped them in the parametrization of the ratio and our fits can describe the data with  $\chi^2/d.o.f. \sim 1$ . Fig. 2 shows a sample plot for 32ID with the unitary pion mass of 174 MeV at  $Q^2 = 0.146 \text{ GeV}^2$ . In view of the fact that the data points are symmetric about  $\tau = t_f/2$ , within uncertainty, it reassures that the sink smearing implemented under the FFT contraction has the same overlap with the pion state as that of the source smearing.

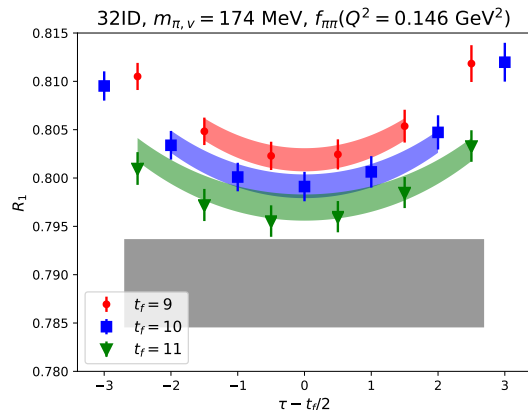


FIG. 2. Example of the ratios of the special  $|\vec{p}_i| = |\vec{p}_f|$  case on 32ID with various values of source-sink separation  $t_f$  and current position  $\tau$ . The data points agree well with the bands predicted from the fit, and the gray band is for the ground state form factor  $f_{\pi\pi}(Q^2)$ .

To obtain  $f_{\pi\pi}(Q^2)$ , we have done a model-independent  $z$ -expansion [44] fit using the following equation with  $k_{\text{max}} \geq 3$ .

$$\begin{aligned}
f_{\pi\pi}(Q^2) &= \sum_{k=0}^{k_{\text{max}}} a_k z^k \\
z(t, t_{\text{cut}}, t_0) &= \frac{\sqrt{t_{\text{cut}} - t} - \sqrt{t_{\text{cut}} - t_0}}{\sqrt{t_{\text{cut}} - t} + \sqrt{t_{\text{cut}} - t_0}},
\end{aligned} \quad (12)$$

where  $t = -Q^2$ , and  $f_{\pi\pi}(0) = 1$  after normalization which leads to the constraint  $a_0 = 1 - \sum_{k=1}^{k_{\text{max}}} a_k z^k(t=0, t_{\text{cut}}, t_0)$ ;  $t_{\text{cut}} = 4m_{\pi, \text{mix}}^2$  corresponds to the two-pion production threshold with  $m_{\pi, \text{mix}}^2 = (m_{\pi, v}^2 + m_{\pi, \text{sea}}^2)/2 + \Delta_{\text{mix}}^{I/D} a^2$ , the partially-quenched pion mass with mixed-action effect included [45],  $m_{\pi, v}$  the valence pion mass and  $m_{\pi, \text{sea}}$  the sea pion mass;  $\Delta_{\text{mix}}^I = 0.041(6) \text{ GeV}^4$  and  $\Delta_{\text{mix}}^{ID} = 0.0105(5) \text{ GeV}^4$ ; and  $t_0$  is chosen to be its “optimal” value  $t_0^{\text{opt}}(Q_{\text{max}}^2) = t_{\text{cut}}(1 - \sqrt{1 + Q_{\text{max}}^2/t_{\text{cut}}})$  to minimize the maximum value of  $|z|$ , with  $Q_{\text{max}}^2$  maximum  $Q^2$  under consideration.

With  $z$ -expansion fitting using Eq. (12), the charge radius of pion can be obtained through the definition in Eq. (2). The  $\langle r_{\pi}^2 \rangle$  on different lattices with different valence pion masses are plotted in Fig. 3. We see that there is a strong dependence on the valence pion masses from the data points on each of the ensembles. Also, from

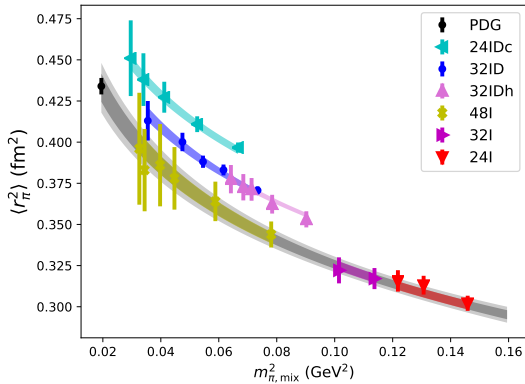


FIG. 3. Pion radius squared  $\langle r_\pi^2 \rangle$  as a function of  $m_{\pi,\text{mix}}^2$ . Data points with different colors correspond to the results on the six ensembles with different sea pion masses.

the comparison of 32ID and 32IDh, we see that the data points line up as a function of  $m_{\pi,\text{mix}}^2$  which evinces a strong dependence on the sea pion mass. The following fitting form as a function of  $m_{\pi,\text{mix}}^2$  is used which includes an essential divergent log term from the  $SU(3)$  NLO ChPT [10, 46],

$$\langle r_\pi^2 \rangle = \langle r_\pi^2 \rangle_{\text{phys}} + b_1 \ln \frac{m_{\pi,\text{mix}}^2}{m_{\pi,\text{phys}}^2} + b_2^{I/ID} a^2 + \frac{b_3 e^{-m_{\pi,\text{mix}} L}}{(m_{\pi,\text{mix}} L)^{3/2}}, \quad (13)$$

where the  $b_1$  term reflects the pion mass dependence,  $m_{\pi,\text{phys}} = 139.57$  MeV is the physical pion mass,  $L$  is the spatial size of the lattice, the  $b_2^{I/ID}$  terms reflect the lattice spacing dependence for the two sets of ensembles with different gauge actions (Iwasaki and Iwasaki plus DSDR), and the  $b_3$  term accounts for the finite volume effect [17, 47, 48]. Since the kaon mass only varies a little in the current pion mass range, we do not include the kaon log term in the fitting. In Fig. 3, the colored bands show our prediction based on the global fit of  $\langle r_\pi^2 \rangle$  with  $\chi^2/d.o.f. = 0.65$ ; the inner gray band shows our prediction for the unitary case of equal pion mass in the valence and the sea in the continuum and infinite volume limits and the outer band includes the systematic uncertainties from excited-state contaminations,  $z$ -expansion fitting, chiral extrapolation, lattice spacing and finite volume dependence. One can see that our prediction of  $\langle r_\pi^2 \rangle = 0.433(9)(13)$  fm<sup>2</sup> at the physical point is in very good agreement with the experimental result (the black dot). The discretization errors across the Iwasaki gauge ensembles are small while those across the Iwasaki plus DSDR gauge ensembles are obvious; this is consistent with what was found in the previous work with the DWF valence quark on similar RBC ensembles [23].

In order to make a prediction of the form factor at the continuum and infinite volume limits, we fit the inverse of the  $f_{\pi\pi}(Q^2)$  data on different lattices with different valence pion masses, as inspired from the NLO  $SU(2)$

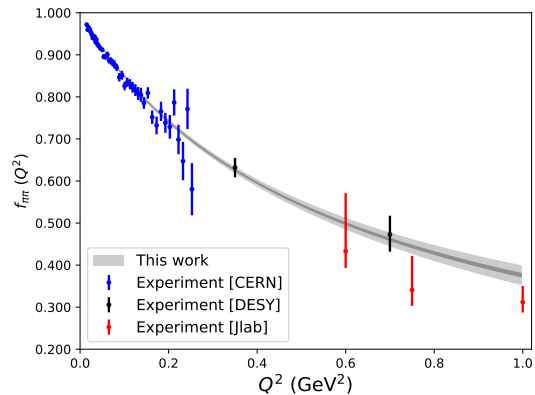


FIG. 4. Comparison of the pion form factor  $f_{\pi\pi}(Q^2)$  at physical pion mass with the CERN experiment at  $Q^2 < 0.25$  GeV<sup>2</sup> [2] and the Jlab and DESY experiment data at larger  $Q^2$  [49–53]. The inner gray band is the statistical error and the outer band includes the systematic uncertainties.

ChPT expansion [9, 10],

$$\frac{1}{f_{\pi\pi}(Q^2)} = 1 + \frac{Q^2}{6(4\pi F_\pi)^2} \left[ \bar{l}_6 - \ln \frac{m_{\pi,\text{mix}}^2}{m_{\pi,\text{phys}}^2} - 1 + R(s) \right] + Q^2 m_{\pi,\text{mix}}^2 (c_1 + c_2 Q^2) + c_3^{I/ID} a^2 Q^2 + c_4^{I/ID} a^2 Q^4 (14) + \frac{Q^2}{(m_{\pi,\text{mix}} L)^{3/2}} (c_5 + c_6 \frac{Q^2}{m_{\pi,\text{mix}}^2}) e^{-M_\pi L},$$

in which  $F_\pi$  and  $\bar{l}_6$  are free parameters for fitting,  $c_1$  and  $c_2$  correspond to possible NNLO effects,  $c_3^{I/ID}$  and  $c_4^{I/ID}$  reflect the lattice spacing dependence terms,  $c_5$  and  $c_6$  correspond to the finite volume effect, and  $R(s) = \frac{2}{3} + (1 + \frac{4}{s}) \left[ \sqrt{1 + \frac{4}{s}} \ln \frac{\sqrt{1 + \frac{4}{s}} - 1}{\sqrt{1 + \frac{4}{s}} + 1} + 2 \right]$ . Since the inverse of  $f_{\pi\pi}(Q^2)$  is mainly dominated by the NLO contributions considering the vector dominance of the pion form factor, fitting the inverse helps avoid the need of too many low-energy constants from NNLO corrections [17]. The mean square charge radius of the pion from this fitting is  $\langle r_\pi^2 \rangle = 0.433(9)$  fm<sup>2</sup>, which is consistent with the above analysis, with  $\chi^2/d.o.f. = 1.0$ . Our extrapolated result at the physical pion mass and continuum and infinite volume limits for the curve  $f_{\pi\pi}(Q^2)$  including the systematic uncertainties from excited-state contaminations, NNLO corrections, chiral extrapolation, lattice spacing and finite volume dependence, is shown and compared with experiments in Fig. 4; it goes through basically all the experimental data points up to  $Q^2 = 1.0$  GeV<sup>2</sup>.

The details of the fitting and the systematic analysis of  $f_{\pi\pi}(Q^2)$  and also  $\langle r_\pi^2 \rangle$  are included in the supplementary materials [43].

**Summary:** We have presented a calculation of the pion form factor using overlap fermions with a range of valence pion masses on six RBC/UKQCD domain-wall ensembles including two which have the physical pion

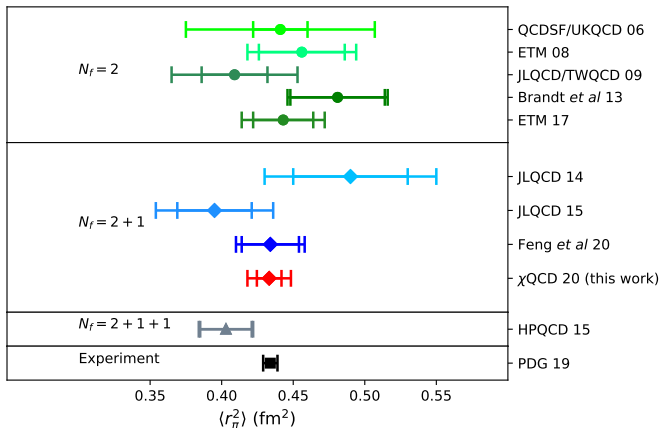


FIG. 5. Summary of the pion radius result at the physical point. The lattice QCD results with different sea flavors are collected in different blocks, while all the results are consistent with each other within uncertainties. Numbers are from (QCDSF/UKQCD) [13], (ETM) [14], (JLQCD/TWQCD) [15], (Brandt et al.) [16], (ETM) [17], (JLQCD) [21, 22], (Feng et al.) [23], (HPQCD) [24], and (PDG) [6].

mass. The lattice results for  $\langle r_\pi^2 \rangle$  in the continuum and infinite volume limits are compiled in Fig. 5 together with that of experiment. Our globally fitted pion mean square charge radius is  $\langle r_\pi^2 \rangle = 0.433(9)(13) \text{ fm}^2$ , which includes systematic errors from chiral extrapolation, finite lattice spacing and others; it agrees with experimental value of  $\langle r_\pi^2 \rangle = 0.434(5) \text{ fm}^2$  within one sigma.

We find that  $\langle r_\pi^2 \rangle$  has a strong dependence on both the valence and sea pion masses. More precisely, it depends majorly on the mass of the pion with one valence quark and one sea quark. We also give the extrapolated form factor  $f_{\pi\pi}(Q^2)$ , and the result agrees well with the

experimental data points (up to  $Q^2 = 1.0 \text{ GeV}^2$ ).

Thus this work shows that the hadron form factor and the corresponding radius can be studied accurately and efficiently by combining LMS with the multi-mass algorithm of overlap fermions and FFT on the stochastic sandwich method, which provides the possibility to investigate the form factor of nucleon and its pion mass dependence with relatively small overhead on multiple quark masses and momentum transfers.

## ACKNOWLEDGMENTS

We thank the RBC/UKQCD Collaborations for providing their domain-wall gauge configurations and also thank L.-C. Jin for constructive discussions. This work is supported in part by the U.S. DOE Grant No. DE-SC0013065 and DOE Grant No. DE-AC05-06OR23177 which is within the framework of the TMD Topical Collaboration. Y.Y is supported by the Strategic Priority Research Program of Chinese Academy of Sciences, Grant No. XDC01040100. This research used resources of the Oak Ridge Leadership Computing Facility at the Oak Ridge National Laboratory, which is supported by the Office of Science of the U.S. Department of Energy under Contract No. DE-AC05-00OR22725. This work used Stampede time under the Extreme Science and Engineering Discovery Environment (XSEDE), which is supported by National Science Foundation Grant No. ACI-1053575. We also thank the National Energy Research Scientific Computing Center (NERSC) for providing HPC resources that have contributed to the research results reported within this paper. We acknowledge the facilities of the USQCD Collaboration used for this research in part, which are funded by the Office of Science of the U.S. Department of Energy.

## SUPPLEMENTARY MATERIALS

### A. Three-point functions fitting

With the usage of Wick contractions and gauge invariance, the three-point function (3pt) with two sources at time slices 0 and  $T/2$  has contributions from the three diagrams shown in Fig. 6. (We assume  $T/2 > t_f > \tau > 0$ .) The diagram 6.(1) contributes

$$C_{3\text{pt},(1)}(\tau, t_f, \vec{p}_i, \vec{p}_f) = \frac{Z_{\vec{p}_i} Z_{\vec{p}_f} (E_i + E_f)}{E_i E_f Z_V} f_{\pi\pi}(Q^2) (e^{-E_i \tau - E_f (t_f - \tau)}) + C_1 e^{-E_i \tau - E_f^1 (t_f - \tau)} + C_2 e^{-E_i^1 \tau - E_f (t_f - \tau)} + C_3 e^{-E_i^1 \tau - E_f^1 (t_f - \tau)}, \quad (15)$$

which includes the first excited-state contaminations, the diagram 6.(2) contributes

$$C_{3\text{pt},(2)}(\tau, t_f, \vec{p}_i, \vec{p}_f) = \frac{Z_{\vec{p}_i} Z_{\vec{p}_f} (E_i + E_f)}{E_i E_f Z_V} f_{\pi\pi}(Q^2) (e^{-E_i (T/2 + \tau) - E_f (t_f - \tau)}), \quad (16)$$

in which we have ignored the excited-state contaminations from the source at  $T/2$  since such terms are suppressed by  $e^{-E_i^1 T/2}$  which is of order  $\sim 10^{-8}$  with  $E_i^1 \approx 1.3 \text{ GeV}$  estimated with the experimental value of the first excited-state

of pion, and the diagram 6.(3) contributes

$$C_{3\text{pt},(3)}(\tau, t_f, \vec{p}_i, \vec{p}_f) = C_4 e^{-E_i(T/2-t_f) - E_h(t_f-\tau)}, \quad (17)$$

in which this term corresponds to the creation of a hadron state with operator  $V_4 = \bar{q}\gamma_4 q$  at time slice  $\tau$  with momentum  $q$  as  $\langle h(q) | V_4 | 0 \rangle$ , an annihilation of a pion state at time slice  $T/2$  with momentum  $p_i$  as  $\langle 0 | \chi_{\pi^+}^\dagger | \pi^-(p_i) \rangle$  and an unknown matrix element  $\langle \pi^-(p_i) | \chi_{\pi^+} | h(q) \rangle$ . The excited-state contaminations from  $E_i^1$  are ignored for the same reason as in the previous discussion and the excited-state contaminations from  $E_h^1$  are ignored under current statistics.

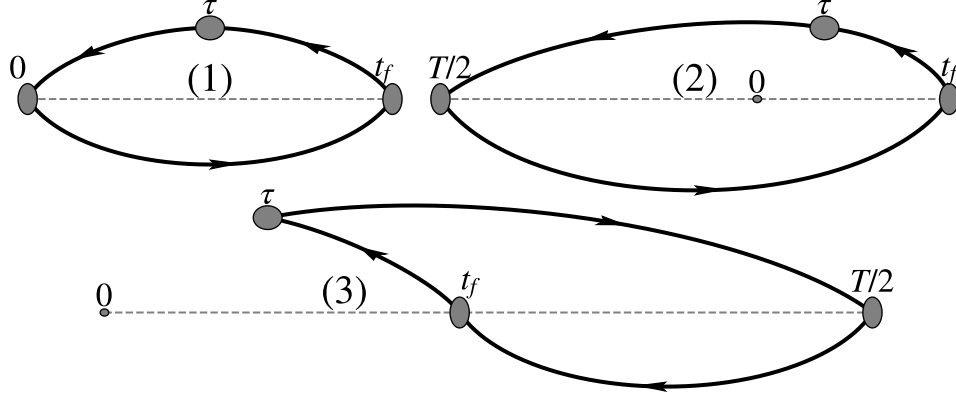


FIG. 6. Diagrams of pion three-point functions with sources at time slices 0 and  $T/2$ .

In order to test the functional form of  $C_{3\text{pt},(3)}(\tau, t_f, \vec{p}_i, \vec{p}_f)$ , we construct 3pt with one source at time slice  $T/2 = 32$  and sink time  $t_f$  at 20, 21, 22 with  $\vec{p}_i = \{0, 0, 0\}$  and  $\vec{p}_f = \{0, 0, \frac{2\pi}{L}\}$ . Then we can evaluate the effective mass  $E_h^{\text{eff}}$  and  $E_i^{\text{eff}}$  from  $C_{3\text{pt},(3)}(\tau, t_f, \vec{p}_i, \vec{p}_f)$  with

$$E_h^{\text{eff}}(\tau, t_f) = \ln \left( \frac{C_{3\text{pt},(3)}(\tau + 1, t_f, \vec{p}_i, \vec{p}_f)}{C_{3\text{pt},(3)}(\tau, t_f, \vec{p}_i, \vec{p}_f)} \right), \quad E_i^{\text{eff}}(\tau, t_f) = \ln \left( \frac{C_{3\text{pt},(3)}(\tau + 1, t_f, \vec{p}_i, \vec{p}_f)}{C_{3\text{pt},(3)}(\tau, t_f - 1, \vec{p}_i, \vec{p}_f)} \right), \quad (18)$$

in which  $E_i^{\text{eff}}$  is evaluated by a simultaneous change of  $\tau$  and  $t_f$  to single out  $E_i$  from exponential  $e^{-E_i(T/2-t_f) - E_h(t_f-\tau)}$ . And they should equal to  $E_h = \sqrt{m_h^2 + (\vec{p}_f - \vec{p}_i)^2}$  and  $E_\pi = \sqrt{m_\pi^2 + \vec{p}_i^2} = m_\pi$  in the  $t_f \gg \tau$  limit, as confirmed in Fig. 7 and the fit results in Fig. 9.

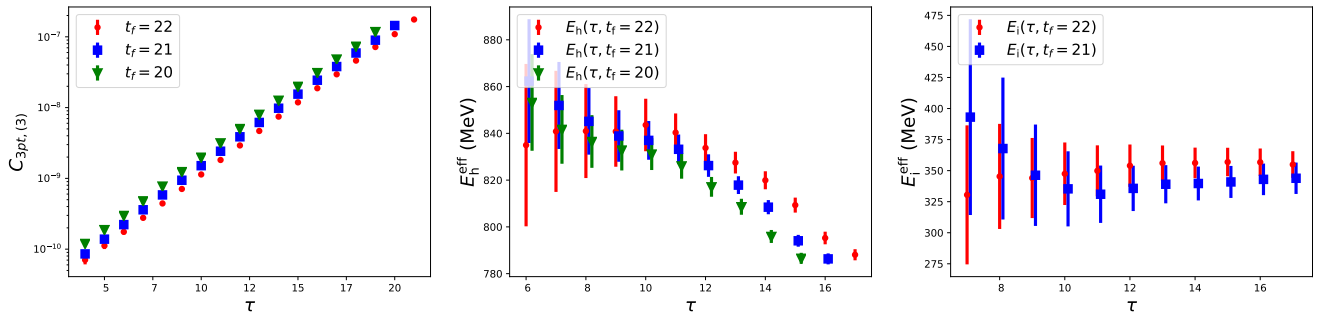


FIG. 7. The plot on the left is of  $C_{3\text{pt},(3)}$  on 24I with  $m_\pi = 347$  MeV, one source at time slice  $T/2$ ,  $\vec{p}_i = \{0, 0, 0\}$  and  $\vec{p}_f = \{0, 0, \frac{2\pi}{L}\}$ . The correlation function is a rising exponential which confirms that  $E_h > 0$  in Eq. (17). The plots in the middle and right panels show the corresponding effective masses  $E_h^{\text{eff}}$  and  $E_i^{\text{eff}}$  obtained with Eq. (18), respectively.

Thus the final functional form is  $C_{3\text{pt}} = C_{3\text{pt},(1)} + C_{3\text{pt},(2)} + C_{3\text{pt},(3)}$  as

$$C_{3\text{pt}}(\tau, t_f, \vec{p}_i, \vec{p}_f) = \frac{Z_{\vec{p}_i} Z_{\vec{p}_f} (E_i + E_f)}{E_i E_f Z_V} f_{\pi\pi}(Q^2) \times (e^{-E_i\tau - E_f(t_f-\tau)} + e^{-E_i(T/2+\tau) - E_f(t_f-\tau)}) \\ + C_1 e^{-E_i\tau - E_f^1(t_f-\tau)} + C_2 e^{-E_i^1\tau - E_f(t_f-\tau)} + C_3 e^{-E_i^1\tau - E_f^1(t_f-\tau)} + C_4 e^{-E_i(T/2-t_f) - E_h(t_f-\tau)}. \quad (19)$$

The associated 2pt is fitted with

$$C_{2pt}(t, \vec{p}) = \frac{Z_{\vec{p}}^2}{E} (e^{-Et} + e^{-E(T-t)} + e^{-E(T/2-t)} + e^{-E(T/2+t)}) + A_1 (e^{-E^1 t} + e^{-E^1(T/2-t)}), \quad (20)$$

with  $A_1$  being a free parameter for the excited-state contributions and the exponential terms with  $T/2$  account for contributions from the source at  $T/2$ . An example of fitted energies is shown in Fig. 8. It can be seen that the first excited-state energy  $E^1$  is close to the experimental value 1.3 GeV and it has been used to constrain the one in 3pt by the joint fit of 2pt and 3pt to extract  $f_{\pi\pi}(Q^2)$ .

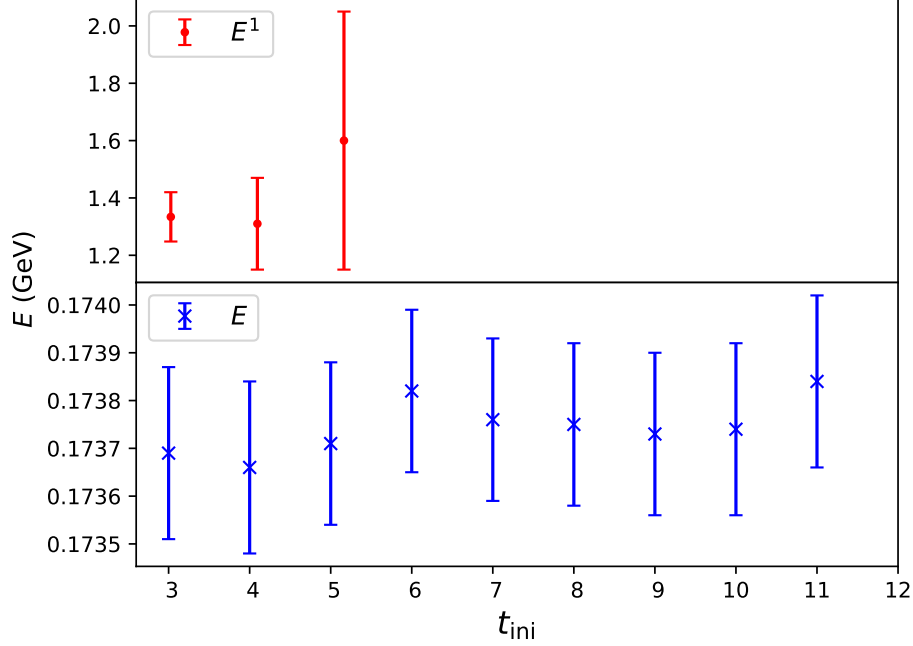


FIG. 8. Pion energies as a function of  $t_{ini}$  with  $[t_{ini}, 15]$  the fit-range of the 2pt on 32ID with pion mass 173.7 MeV at zero momentum. The contributions from the first excited state are ignored for  $t_{ini} \geq 6$  under current statistics.

In order to test the fitting function of 3pt in Eq. (19), a comparison of the fitting of the one-source result with the source at  $t = 0$  and that of the two-source result with sources at  $t = 0$  and 32 in the same inversion is shown in Fig. 9. For illustrative purpose, the data points are shown with ratio  $R_2$ ,

$$\begin{aligned} R_2(\tau, t_f, \vec{p}_i, \vec{p}_f) &= \frac{C_{3pt}(\tau, t_f, \vec{p}_i, \vec{p}_f)}{\frac{Z_{\vec{p}_i} Z_{\vec{p}_f} (E_i + E_f)}{4E_i E_f Z_V} (e^{-E_i \tau - E_f(t_f - \tau)} + e^{-E_i(T/2 + \tau) - E_f(t_f - \tau)})} \\ &= f_{\pi\pi}(Q^2) + \text{excited-state terms} + C_4 \text{ term}, \end{aligned} \quad (21)$$

in which  $Z_{\vec{p}}$  and  $E$  are determined from the fitting of 2pt and  $Z_V$  from 3pt at zero momentum transfer. It can be seen that the two results agree with each other within 2pc uncertainty which again confirms our fitting formula.

Thus for the general momentum setup  $|\vec{p}_i| \neq |\vec{p}_f|$  we can proceed further to fit  $C_{3pt}(\tau, t_f, \vec{p}_i, \vec{p}_f)$  together with  $C_{3pt}(\tau, t_f, \vec{p}_i, \vec{p}_i)$  which corresponds to the exchange of initial and final momentum. Fig. 10 shows example plots on 24IDc and 32ID. The data points are fitted well with Eq. (19) and the fit results are shown in bands with  $\chi^2/d.o.f. \sim 1$ . The data points for  $C_{3pt}(\tau, t_f, \vec{p}, \vec{0})$  are lower and closer to the gray band since the  $C_4$  term has negative contribution with a suppression factor  $e^{-E(\vec{p})T/2}$  compared to the case of  $C_{3pt}(\tau, t_f, \vec{0}, \vec{p})$  in which the  $C_4$  term has positive and large contribution with only a suppression factor  $e^{-E(\vec{0})T/2}$ .

## B. $z$ -expansion fit and chiral extrapolation of pion radius

In order to remove the model dependence of the  $z$ -expansion fitting, we need to take  $k_{max}$  to be large enough such that the fit results are independent of the precise value of  $k_{max}$ . One way of achieving this is putting a Gaussian

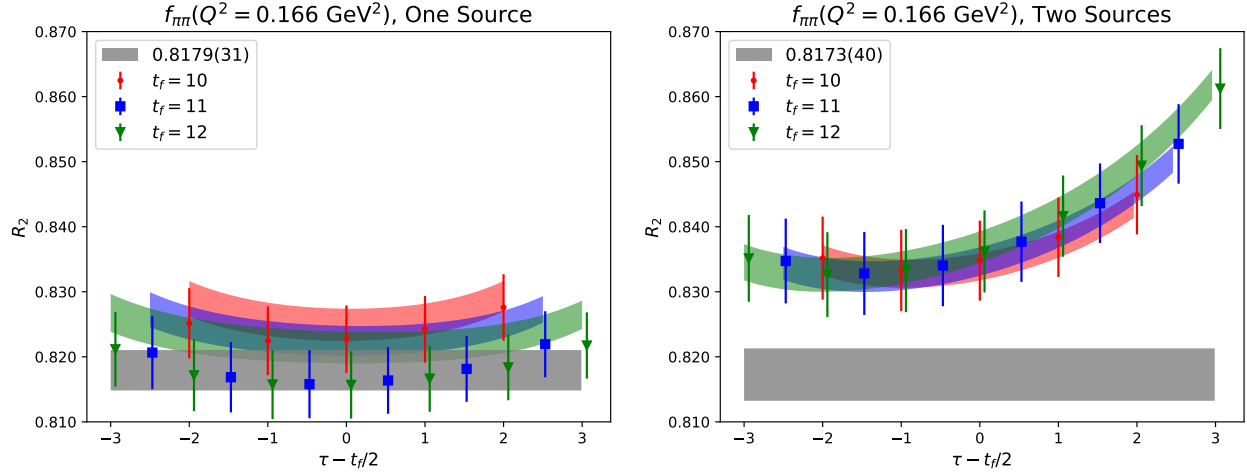


FIG. 9. Joint fitting results on 24I with  $m_\pi = 347$  MeV,  $\vec{p}_i = \{0, 0, 0\}$  and  $\vec{p}_f = \{0, 0, \frac{2\pi}{L}\}$ . The plot on the left corresponds to the case of one source at time slice 0. The gray band is for the ground state form factor  $f_{\pi\pi}(Q^2)$  which is close to the data points due to small excited-state contaminations. The plot on the right corresponds to the case of a source at each of the time slices 0 and  $T/2$ . The gray band is far away from the rising data points due to the additional  $C_4$  term with fitted  $E_h = 807(82)$  MeV which is consistent with the result of Fig. 7.

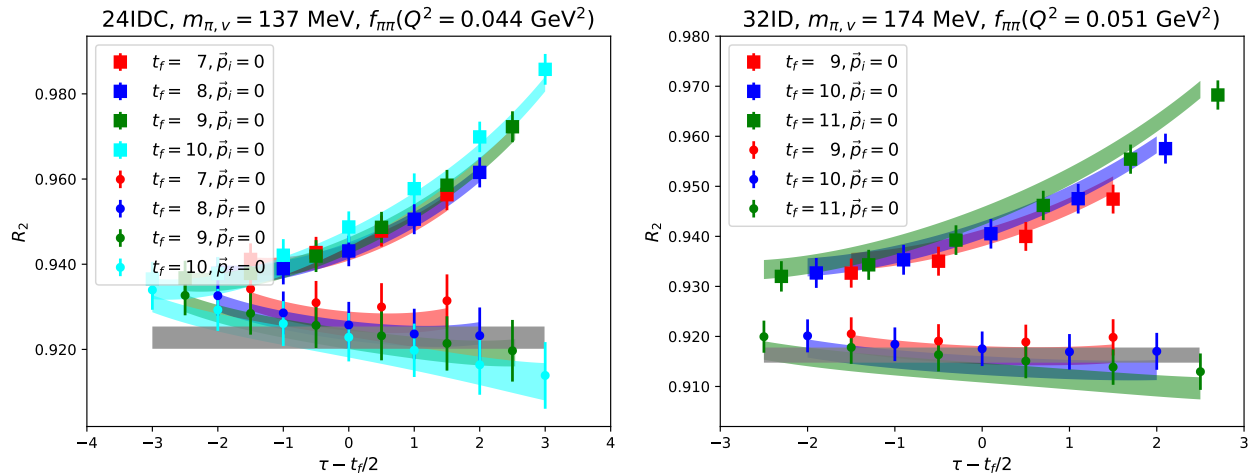


FIG. 10. Examples of the ratios on 24IDc and 32ID with various values of source-sink separation  $t_f$  and current position  $\tau$ . The plots show the general  $|\vec{p}_i| \neq |\vec{p}_f|$  case with square points  $\vec{p}_i = -\vec{q}, \vec{p}_f = 0$  and dot points  $p_i = 0, \vec{p}_f = \vec{q}$ . The data points agree well with the bands predicted from the fit, and the gray band is for the ground state form factor  $f_{\pi\pi}(Q^2)$ .

bound on the  $z$ -expansion  $a_k$  with central value 0. The choice of the Gaussian bound can be investigated using the Vector Meson Dominance (VMD) model with rho meson mass  $m_\rho = 775$  MeV,

$$f_{\pi\pi}(Q^2) = \frac{1}{1 + Q^2/m_\rho^2}. \quad (22)$$

A non-linear least squares fit of this analytical function with  $z$ -expansion fitting at  $k_{\max} = 10$  gives  $|a_k/a_0|_{\max} < 1.03$ , in which we used  $t_{\text{cut}} = 4m_{\pi,\text{phys}}^2$ ,  $t_0^{\text{opt}}(Q_{\max}^2) = t_{\text{cut}}(1 - \sqrt{1 + Q_{\max}^2/t_{\text{cut}}})$  and  $Q_{\max}^2 = 1.0$  GeV<sup>2</sup>. Also by investigating the  $z$ -expansion fits with  $k_{\max} = 3$  without priors of our data, we find  $|a_k/a_0|_{\max} < 3.0$ . Thus we propose the use of conservative choice of Gaussian bound [44] with  $|a_k/a_0|_{\max} = 5$  for the pion form factor. The  $z$ -expansion fitted pion form factors up to  $Q^2 \sim 1.0$  GeV<sup>2</sup> for the six lattices with the same valence and sea pion mass are shown in Fig. 11 with  $\chi^2/d.o.f. \sim [0.4, 0.9]$ .

Another way to reach higher  $k_{\max}$  and control the model dependence of fittings is using the fact that at the  $Q^2 \rightarrow \infty$  limit  $f_{\pi\pi}(Q^2)$  falls as  $1/Q^2$  up to logarithms [54, 55]. Thus we have  $Q^k f_{\pi\pi}(Q^2) \rightarrow 0$  for  $k = 0, 1$  and follow the same

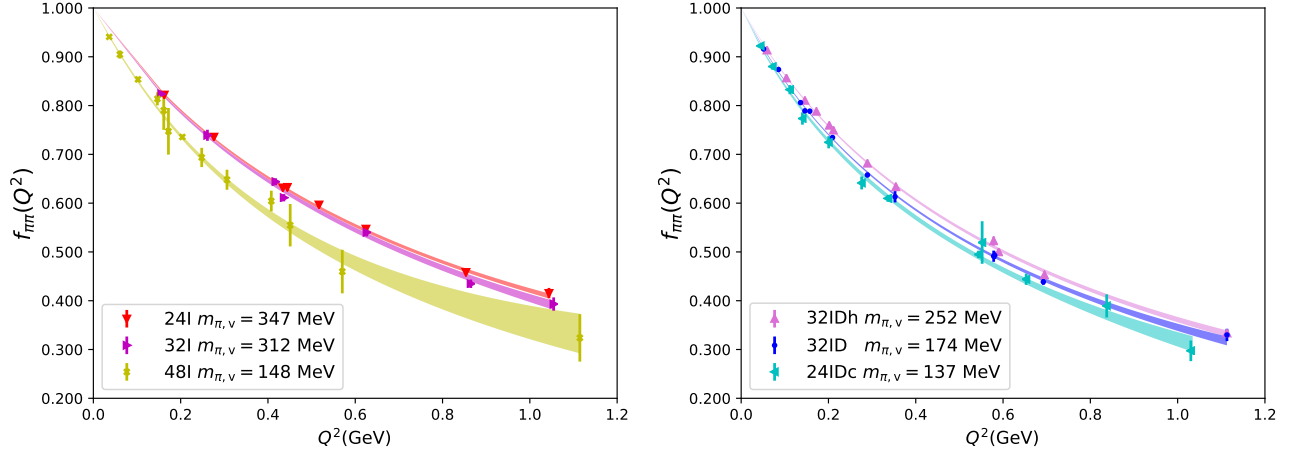


FIG. 11.  $z$ -expansion fitting of the pion form factors on six gauge ensembles at their unitary pion mass with  $k_{\max} = 3$  and  $|a_k/a_0|_{\max} = 5$ . The left panel is for the ensembles using Iwasaki gauge action and the Iwasaki+DSDR cases are shown in the right panel.

argument in [44], this implies

$$\left. \frac{d^n}{dz^n} f_{\pi\pi} \right|_{z=1} = 0, \quad n = 0, 1, \quad (23)$$

with  $z = 1$  corresponding to the  $Q^2 \rightarrow \infty$  limit. These equations will lead to the two sum rules for pion form factors as

$$\sum_{k=0}^{\infty} a_k = 0, \quad \sum_{k=1}^{\infty} k a_k = 0. \quad (24)$$

The estimates of the extrapolated charge radius of the pion using

$$\langle r_{\pi}^2 \rangle = \langle r_{\pi}^2 \rangle_{\text{phys}} + b_1 \ln \frac{m_{\pi, \text{mix}}^2}{m_{\pi, \text{phys}}^2} + b_2^{I/ID} a^2 + \frac{b_3 e^{-m_{\pi, \text{mix}} L}}{(m_{\pi, \text{mix}} L)^{3/2}}, \quad (25)$$

with different  $z$ -expansion fits are shown in Fig. 12. Since  $b_2^I$  and  $b_3$  have no statistical significance, we use only three free parameters  $\langle r_{\pi}^2 \rangle_{\text{phys}}$ ,  $b_1$  and  $b_2^{I/ID}$  in these fits. All the fits have good  $\chi^2/d.o.f. \sim 0.6$  with the central values and error values varying a little. Thus we take the result shown in black  $\langle r_{\pi}^2 \rangle = 0.4332(86) \text{ fm}^2$  which corresponds to  $k_{\max} = 3$  and  $|a_k/a_0|_{\max} = 5$  as our fit result. The systematic uncertainties considered are listed as follows:

- The maximum difference between the result shown in black in Fig. 12 with the other fitted cases is treated as the systematic uncertainty from  $z$ -expansion fitting.
- The systematic uncertainty from the excited-state contaminations is estimated by changing the fit-ranges of 2pt and 3pt on 32ID with pion mass 174 MeV at the smallest momentum transfer which results in  $f_{\pi\pi}(Q^2 = 0.051 \text{ GeV}^2) = 0.9158(14)(13)$ ; the second error corresponds to the systematic uncertainty from excited-state contaminations. This case is chosen because of its good signal/noise ratio which has the most control of the final result at close to physical pion mass and the smallest momentum transfer is chosen due to its largest influence on the radius. In order to estimate the systematic uncertainty of the radius from the form factor at only one small momentum transfer, we solve VMD model in Eq. (22),

$$\frac{1}{1 + (0.051 \text{ GeV}^2)/m_{\rho}} = 0.9158(14)(13) \quad (26)$$

with  $m_{\rho}$  as a free parameter. The predicted radius is  $\langle r_{\pi}^2 \rangle = 6.0/m_{\rho} = 0.4190(74)(68) \text{ fm}^2$ . The second error  $0.0068 \text{ fm}^2$ , which propagates from the systematic uncertainty of the form factor, is treated as the systematic uncertainty from the change of fit ranges for the extrapolated charge radius.

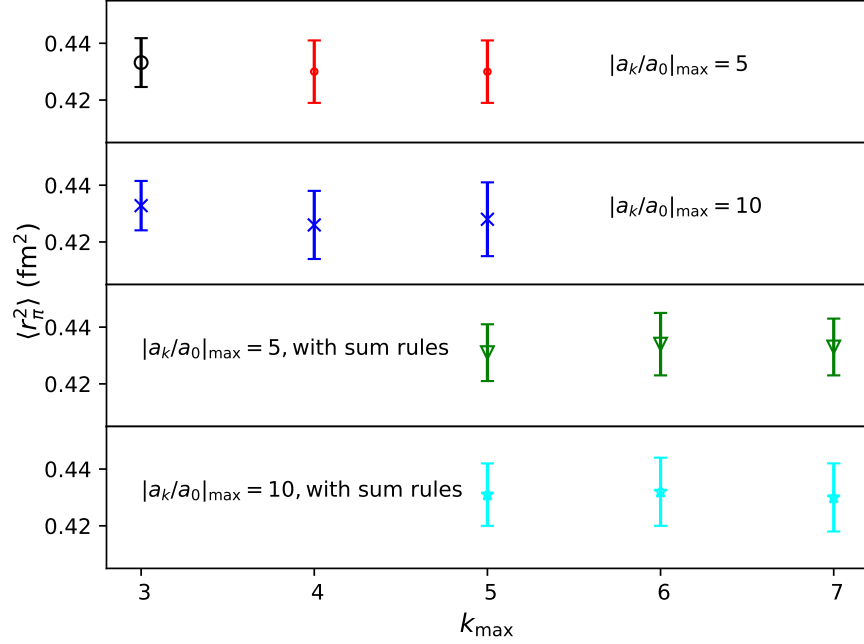


FIG. 12. Comparison of extrapolated  $\langle r_\pi^2 \rangle$  with  $z$ -expansion fits with different  $k_{\max}$ . The first and second sets are the fits with priors  $|a_k/a_0|_{\max} = 5$  and  $|a_k/a_0|_{\max} = 10$ , respectively. The third and fourth sets are the similar fits along with the sum rules in Eq. (24).

- We added a linear dependence term between the charge radius of the pion and the pion mass squared as  $b_4 M_\pi^2$  to Eq. (25) proposed by SU(2) NNLO ChPT [9] and repeated the fit with four free parameters  $\langle r_\pi^2 \rangle_{\text{phys}}$ ,  $b_1$ ,  $b_2^{ID}$  and  $b_4$ . The coefficient  $b_4$  is consistent with zero and the prediction changed by  $0.0032 \text{ fm}^2$  which is treated as the chiral extrapolation systematic uncertainty.

Another source of the chiral extrapolation systematic uncertainty is the lack of kaon log term in Eq. (25). On 24I, the valence pion masses ranging from 256 MeV to 391 MeV gives a range of kaon mass from 514 MeV to 554 MeV. Thus we estimate the maximum kaon mass for the pion mass range in consideration to be  $M_{K,\max} = 554 \text{ MeV}$ . With the usage of SU(3) NLO ChPT [10], the systematic uncertainty from the kaon log term can be given by  $\frac{1}{32\pi^2 F_0^2} \ln \frac{M_{K,\max}^2}{M_{K,p}^2} = 0.0026 \text{ fm}^2$ , in which  $F_0 = 93.3 \text{ MeV}$  and  $M_{K,p} = 493 \text{ MeV}$  is the physical kaon mass.

- We repeated the fitting with four free parameters  $\langle r_\pi^2 \rangle_{\text{phys}}$ ,  $b_1$ ,  $b_2^{ID}$  and  $b_2^I$  which includes the discretization error from the Iwasaki gauge action and the prediction changed by  $0.0025 \text{ fm}^2$ . With this fitting, we get a difference between the fitting predictions in the continuum limit with those from the smallest lattice spacing (32I) to be  $0.0018 \text{ fm}^2$ . We combined these two as the systematic uncertainty of finite lattice spacing.
- With similar systematic analysis for finite volume effects with four free parameters  $\langle r_\pi^2 \rangle_{\text{phys}}$ ,  $b_1$ ,  $b_2^{ID}$  and  $b_3$ , the prediction changed by  $0.0058 \text{ fm}^2$  and the difference between the fitting predictions in the infinite volume limit with those from the largest  $m_\pi L = 5.8$  (32IDh) in our simulation is negligible.

Thus, the final result of the mean square charge radius of the pion at the physical pion mass in the physical limit reads

$$\langle r_\pi^2 \rangle = 0.4332(86)_{\text{stat}}(72)_{z\text{-exp}}(68)_{\text{fit-range}}(41)_\chi(31)_a(58)_V \text{ fm}^2 = 0.4332(86)(125) \text{ fm}^2, \quad (27)$$

with statistical error (stat), systematic uncertainty from  $z$ -expansion fitting ( $z$ -exp), fit-range dependence (fit-range), chiral extrapolation ( $\chi$ ), finite lattice spacing (a), and finite volume (V). The total uncertainties at heavier pion masses are estimated from the scale of the total/statistical ratio at the physical pion mass.

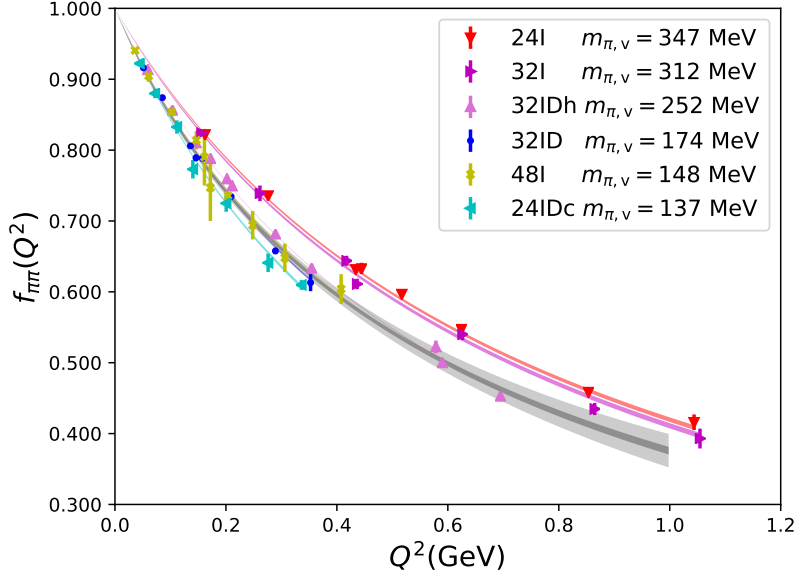


FIG. 13. Pion form factor  $f_{\pi\pi}(Q^2)$  on six gauge ensembles at their unitary pion mass with the bands from the chiral extrapolation fitting. The inner gray error band shows the fitting result and statistical error extrapolated to the physical limit and the outer band corresponds to the inclusion of the systematic uncertainties from excited-state contaminations, NNLO corrections, chiral extrapolation, lattice spacing and finite volume dependence.

### C. Chiral extrapolation of pion form factor

The fitting result of the chiral extrapolation of the pion form factor with

$$\begin{aligned} \frac{1}{f_{\pi\pi}(Q^2)} = & 1 + \frac{Q^2}{6(4\pi F_\pi)^2} \left[ \bar{l}_6 - \ln \frac{m_{\pi,\text{mix}}^2}{m_{\pi,\text{phys}}^2} - 1 + R(s) \right] + Q^2 m_{\pi,\text{mix}}^2 (c_1 + c_2 Q^2) \\ & + c_3^{I/ID} a^2 Q^2 + c_4^{I/ID} a^2 Q^4 + \frac{Q^2}{(m_{\pi,\text{mix}} L)^{3/2}} (c_5 + c_6 \frac{Q^2}{m_{\pi,\text{mix}}^2}) e^{-M_\pi L}, \end{aligned} \quad (28)$$

is shown in Fig. 13. We have made a cut of the  $Q^2$  ranges used on each ensembles with  $Q^2/m_{\pi,\text{mix}}^2 < 13$ , so that the current formula can fully describe our data without the need of higher order terms of the ChPT expansion. The following systematic uncertainties are included in the analysis:

- With a variation of the fit-ranges of 2pt and 3pt on 32I with pion mass 312 MeV we got the form factor at large momentum transfer  $f_{\pi\pi}(Q^2 = 0.865 \text{ GeV}^2) = 0.4347(87)(98)$ . Along with previous analysis on 32ID at small momentum transfer  $f_{\pi\pi}(Q^2 = 0.051 \text{ GeV}^2) = 0.9158(14)(13)$ , we estimate the systematic uncertainty from the excited-state contaminations to be equal to the statistical uncertainty of the fitted pion form factors for all  $Q^2 < 1.0 \text{ GeV}^2$ .
- Since the  $c_1$  and  $c_2$  terms are just an estimation of the possible NNLO effects, we estimate the NNLO systematic uncertainty by setting  $c_1$  and  $c_2$  in Eq. (28) to be zero and treat the changes as systematic uncertainty from NNLO corrections.
- The systematic uncertainty from the lack of a kaon log term proposed by  $SU(3)$  NLO ChPT is calculated with

$$\frac{Q^2}{12(4\pi F_0)^2} \left[ \ln \frac{M_{K,\text{max}}^2}{m_{K,p}^2} \right], \quad (29)$$

which is the difference between using  $M_{K,\text{max}}$  and  $m_{K,p}$  in the ChPT formula. This is treated as the systematic uncertainty from chiral extrapolation.

- We use the difference between the fitting predictions in the continuum limit with those from the smallest lattice spacing (32I) as systematic uncertainty of finite lattice spacing.

- The systematic uncertainty from finite volume effects is estimated by the difference between the fitting predictions in the infinite volume limit with those from the largest  $m_\pi L = 5.8$  (32IDh).

- 
- [1] E. Dally *et al.*, *Phys. Rev. Lett.* **48**, 375 (1982).
- [2] S. Amendolia *et al.* (NA7), *Nucl. Phys. B* **277**, 168 (1986).
- [3] I. M. Gough Eschrich *et al.* (SELEX), *Phys. Lett. B* **522**, 233 (2001), [arXiv:hep-ex/0106053](#).
- [4] B. Ananthanarayan, I. Caprini, and D. Das, *Phys. Rev. Lett.* **119**, 132002 (2017), [arXiv:1706.04020 \[hep-ph\]](#).
- [5] G. Colangelo, M. Hoferichter, and P. Stoffer, *JHEP* **02**, 006 (2019), [arXiv:1810.00007 \[hep-ph\]](#).
- [6] M. Tanabashi *et al.* (Particle Data Group), *Phys. Rev. D* **98**, 030001 (2018).
- [7] W. R. Frazer and J. R. Fulco, *Phys. Rev.* **117**, 1609 (1960).
- [8] W. Holladay, *Phys. Rev.* **101**, 1198 (1956).
- [9] J. Gasser and H. Leutwyler, *Nucl. Phys. B* **250**, 517 (1985).
- [10] J. Bijnens, G. Colangelo, and P. Talavera, *JHEP* **05**, 014 (1998), [arXiv:hep-ph/9805389](#).
- [11] G. Martinelli and C. T. Sachrajda, *Nucl. Phys. B* **306**, 865 (1988).
- [12] T. Draper, R. Woloshyn, W. Wilcox, and K.-F. Liu, *Nucl. Phys. B* **318**, 319 (1989).
- [13] D. Brmmel *et al.* (QCDSF/UKQCD), *Eur. Phys. J. C* **51**, 335 (2007), [arXiv:hep-lat/0608021](#).
- [14] R. Frezzotti, V. Lubicz, and S. Simula (ETM), *Phys. Rev. D* **79**, 074506 (2009), [arXiv:0812.4042 \[hep-lat\]](#).
- [15] S. Aoki *et al.* (JLQCD, TWQCD), *Phys. Rev. D* **80**, 034508 (2009), [arXiv:0905.2465 \[hep-lat\]](#).
- [16] B. B. Brandt, A. Jttner, and H. Wittig, *JHEP* **11**, 034 (2013), [arXiv:1306.2916 \[hep-lat\]](#).
- [17] C. Alexandrou *et al.* (ETM), *Phys. Rev. D* **97**, 014508 (2018), [arXiv:1710.10401 \[hep-lat\]](#).
- [18] F. D. Bonnet, R. G. Edwards, G. T. Fleming, R. Lewis, and D. G. Richards (Lattice Hadron Physics), *Phys. Rev. D* **72**, 054506 (2005), [arXiv:hep-lat/0411028](#).
- [19] P. Boyle, J. Flynn, A. Juttner, C. Kelly, H. de Lima, C. Maynard, C. Sachrajda, and J. Zanotti, *JHEP* **07**, 112 (2008), [arXiv:0804.3971 \[hep-lat\]](#).
- [20] O. H. Nguyen, K.-I. Ishikawa, A. Ukawa, and N. Ukita, *JHEP* **04**, 122 (2011), [arXiv:1102.3652 \[hep-lat\]](#).
- [21] H. Fukaya, S. Aoki, S. Hashimoto, T. Kaneko, H. Matsu-furu, and J. Noaki, *Phys. Rev. D* **90**, 034506 (2014), [arXiv:1405.4077 \[hep-lat\]](#).
- [22] S. Aoki, G. Cossu, X. Feng, S. Hashimoto, T. Kaneko, J. Noaki, and T. Onogi (JLQCD), *Phys. Rev. D* **93**, 034504 (2016), [arXiv:1510.06470 \[hep-lat\]](#).
- [23] X. Feng, Y. Fu, and L.-C. Jin, *Phys. Rev. D* **101**, 051502 (2020), [arXiv:1911.04064 \[hep-lat\]](#).
- [24] J. Koponen, F. Bursa, C. Davies, R. Dowdall, and G. Lepage, *Phys. Rev. D* **93**, 054503 (2016), [arXiv:1511.07382 \[hep-lat\]](#).
- [25] A. Li *et al.* (xQCD), *Phys. Rev. D* **82**, 114501 (2010), [arXiv:1005.5424 \[hep-lat\]](#).
- [26] Y.-B. Yang, J. Liang, Y.-J. Bi, Y. Chen, T. Draper, K.-F. Liu, and Z. Liu, *Phys. Rev. Lett.* **121**, 212001 (2018), [arXiv:1808.08677 \[hep-lat\]](#).
- [27] Y.-B. Yang, R. S. Sufian, A. Alexandru, T. Draper, M. J. Glatzmaier, K.-F. Liu, and Y. Zhao, *Phys. Rev. Lett.* **118**, 102001 (2017), [arXiv:1609.05937 \[hep-ph\]](#).
- [28] J. W. Cooley and J. W. Tukey, *Mathematics of Computation* **19**, 297 (1965).
- [29] Y. Aoki *et al.* (RBC, UKQCD), *Phys. Rev. D* **83**, 074508 (2011), [arXiv:1011.0892 \[hep-lat\]](#).
- [30] T. Blum *et al.* (RBC, UKQCD), *Phys. Rev. D* **93**, 074505 (2016), [arXiv:1411.7017 \[hep-lat\]](#).
- [31] P. Boyle *et al.*, *Phys. Rev. D* **93**, 054502 (2016), [arXiv:1511.01950 \[hep-lat\]](#).
- [32] T.-W. Chiu, *Phys. Rev. D* **60**, 034503 (1999), [arXiv:hep-lat/9810052](#).
- [33] K.-F. Liu, *Int. J. Mod. Phys. A* **20**, 7241 (2005), [arXiv:hep-lat/0206002](#).
- [34] T.-W. Chiu and S. V. Zenkin, *Phys. Rev. D* **59**, 074501 (1999), [arXiv:hep-lat/9806019](#).
- [35] T. A. DeGrand and R. D. Loft, *Comput. Phys. Commun.* **65**, 84 (1991).
- [36] C. Allton, C. T. Sachrajda, V. Lubicz, L. Maiani, and G. Martinelli, *Nucl. Phys. B* **349**, 598 (1991).
- [37] J. Liang, Y.-B. Yang, K.-F. Liu, A. Alexandru, T. Draper, and R. S. Sufian, *Phys. Rev. D* **96**, 034519 (2017), [arXiv:1612.04388 \[hep-lat\]](#).
- [38] S.-J. Dong and K.-F. Liu, *Phys. Lett. B* **328**, 130 (1994), [arXiv:hep-lat/9308015](#).
- [39] C. W. Bernard, T. Draper, G. Hockney, A. Rushton, and A. Soni, *Phys. Rev. Lett.* **55**, 2770 (1985).
- [40] G. Martinelli and C. T. Sachrajda, *Nucl. Phys. B* **316**, 355 (1989).
- [41] Y.-B. Yang, A. Alexandru, T. Draper, M. Gong, and K.-F. Liu, *Phys. Rev. D* **93**, 034503 (2016), [arXiv:1509.04616 \[hep-lat\]](#).
- [42] J. Liang, Y.-B. Yang, T. Draper, M. Gong, and K.-F. Liu, *Phys. Rev. D* **98**, 074505 (2018), [arXiv:1806.08366 \[hep-ph\]](#).
- [43] Supplemental materials.
- [44] G. Lee, J. R. Arrington, and R. J. Hill, *Phys. Rev. D* **92**, 013013 (2015), [arXiv:1505.01489 \[hep-ph\]](#).
- [45] M. Lujan, A. Alexandru, Y. Chen, T. Draper, W. Freeman, M. Gong, F. Lee, A. Li, K. Liu, and N. Mathur, *Phys. Rev. D* **86**, 014501 (2012), [arXiv:1204.6256 \[hep-lat\]](#).
- [46] D. Arndt and B. C. Tiburzi, *Phys. Rev. D* **68**, 094501 (2003), [arXiv:hep-lat/0307003](#).
- [47] T. Bunton, F.-J. Jiang, and B. Tiburzi, *Phys. Rev. D* **74**, 034514 (2006), [Erratum: *Phys.Rev.D* 74, 099902 (2006)], [arXiv:hep-lat/0607001](#).
- [48] F.-J. Jiang and B. Tiburzi, *Phys. Lett. B* **645**, 314 (2007), [arXiv:hep-lat/0610103](#).
- [49] G. Huber *et al.* (Jefferson Lab), *Phys. Rev. C* **78**, 045203 (2008), [arXiv:0809.3052 \[nucl-ex\]](#).

- [50] H. Blok *et al.* (Jefferson Lab), *Phys. Rev. C* **78**, 045202 (2008), [arXiv:0809.3161 \[nucl-ex\]](#).
- [51] T. Horn *et al.*, *Phys. Rev. C* **78**, 058201 (2008), [arXiv:0707.1794 \[nucl-ex\]](#).
- [52] T. Horn *et al.* (Jefferson Lab F(pi)-2), *Phys. Rev. Lett.* **97**, 192001 (2006), [arXiv:nucl-ex/0607005](#).
- [53] J. Volmer *et al.* (Jefferson Lab F(pi)), *Phys. Rev. Lett.* **86**, 1713 (2001), [arXiv:nucl-ex/0010009](#).
- [54] G. Lepage and S. J. Brodsky, *Phys. Lett. B* **87**, 359 (1979).
- [55] G. R. Farrar and D. R. Jackson, *Phys. Rev. Lett.* **43**, 246 (1979).